Electronic Supplementary Information

Combining $Ti_4(embonate)_6$ Anionic Cage and π-Conjugated Coordination Cation for Highly Effective Optical Limiting

Yuan Yuan [a,b], Dong-Hui Zhang [a,b], Qiao-Hong Li [b], Shu-Mei Chen [a,*], Yan-Ping He [b,*] and Jian Zhang [b,*]

[a] College of Chemistry, Fuzhou University, Fuzhou, Fujian 350108, P. R. China.

[b] State Key Laboratory of Structural Chemistry, Fujian Institute of Research on the Structure of Matter, Chinese Academy of Sciences, Fuzhou, Fujian 350002, P. R. China.

* Corresponding Author: csm@fzu.edu.cn; hyp041@163.com; zhj@fjirsm.ac.cn

1. Experimental section.

Materials and instrumentation: All the reagents and solvents employed are purchased commercially and used as received without further treatment.Ligands were purchased commercially. All syntheses were carried out in a 20 mL vial under autogenous pressure. Thermogravimetric (TGA) analysis was performed on a Netzch STA449F3 analyzer at a heating rate of 10 ℃/min from ambient temperature to 800 ℃ under N_2 atmosphere. Powder XRD was recorded on a Rigaku Dmax/2500 X-ray diffractometer operating at 40 kV and 100 mA, using Ga-Kα radiation(λ = 1.3405 Å). The patterns were scanned over an angular range of 3–50 ° (2 theta) with a step length of 0.05 ° (2 theta). The UV diffuse reflection data were recorded at room temperature using a powder sample with $BaSO_4$ as a standard (100% reflectance) on a PerkinElmer Lamda-950 UV spectrophotometer.

Synthesis of $[(Me_2NH_2)_8(Ti_4L_6)]$ *Guests* (PTC-101). PTC-101 as a starting material of Ti_4L_6 cages was massively synthesized by the method reported in our previous work.[1] Ti(O*i*Pr)$_4$ (160 μL, 0.50 mmol), H_4L (embonate) (155 mg, 0.40 mmol), and 2 drops of ethylenediamine (en) were added to 6 mL of *n*-propanol/DMF (3:1 v/v) and mixed at room temperature. The resultant solution was heated at 100 ℃ for 3 days. After the reaction mixture was cooled to room temperature, red crystals of PTC-101 were obtained. (Yield: 82% based on L.).

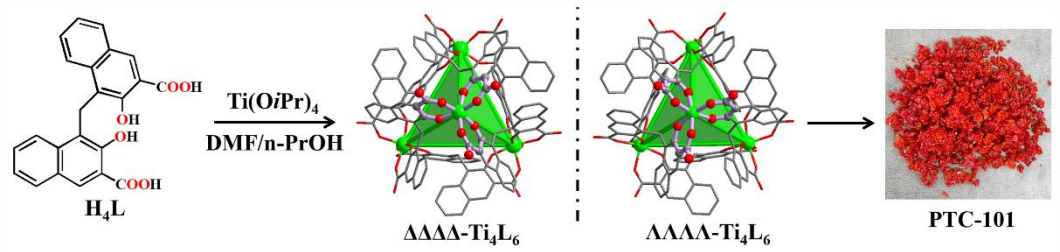

Scheme S1. The synthetic route of $(Ti_4L_6)^{8-}$ cage precursor.

Synthesis of $\{(Me_2CH_2)_2[Ag_2(phen)_2(dppm)]_3(Ti_4L_6)\}$ *Guests* (PTC-379). PTC-101 (80 mg, 0.02 mmol), Ag(OAc) (15 mg, 0.09 mmol), bis(diphenylphosphino)methane (dppm) (30 mg, 0.08 mmol), 1,10-phenanthroline (phen) (15 mg, 0.08 mmol) were dissolved in 6 mL of NMF/H_2O (2:1 v/v, NMF=formamide) mixed at room temperature. The mixture was heated at 80 ℃ for 3 days. After cooled to room temperature, red crystals of **PTC-379** were synthesized. (Yield: 30% based on PTC-101).

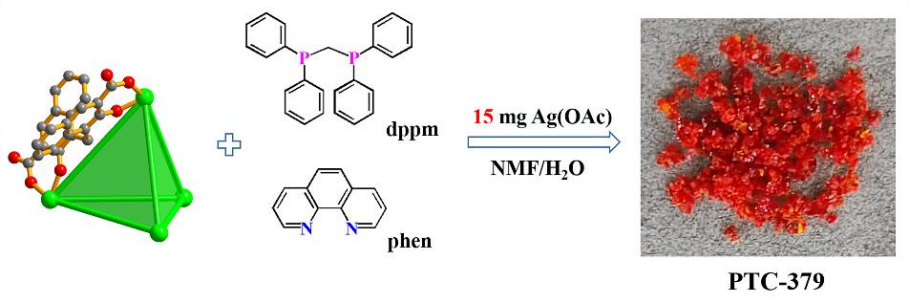

Scheme S2. The synthetic route of **PTC-379**.

Synthesis of {$(Me_2CH_2)_6[Ag_2(phen)_2(dppm)_2](Ti_4L_6)$} *Guests* (PTC-380). PTC-101 (80 mg, 0.02 mmol), Ag(OAc) (30 mg, 0.18 mmol), dppm (30 mg, 0.08mmol), phen (15 mg, 0.08 mmol) were dissolved in 6 mL of NMF/H_2O (2:1 v/v, NMF = formamide) mixed at room temperature. The mixture was heated at 80 ℃ for 3 days. After cooled to room temperature, red crystals of **PTC-380** were synthesized. (Yield: 35% based on PTC-101).

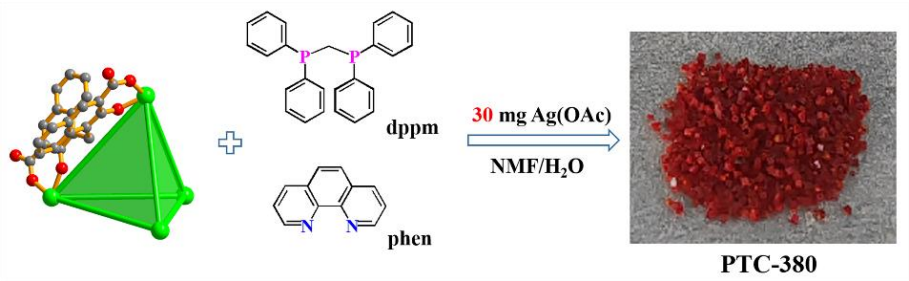

Scheme S3. The synthetic route of **PTC-380**.

Synthesis of {$[Ag_2(S\text{-}dpen)(dppm)]_4(Ti_4L_6)$} *Guests* (PTC-381). PTC-101 (80 mg, 0.02 mmol), Ag(OAc) (30 mg, 0.18 mmol), dppm (30 mg, 0.08 mmol), (1S,2S)-(-)-1,2-diphenyl-1,2-ethanediamine (S-dpen) (30mg, 0.14 mmol) were dissolved in 6 mL of H_2O/THF (1:1 v/v) and mixed at room temperature. The mixture was heated at 80 ℃ for 3 days. After cooled to room temperature, yellow crystals of **PTC-381** were synthesized. (Yield: 40% based on PTC-101).

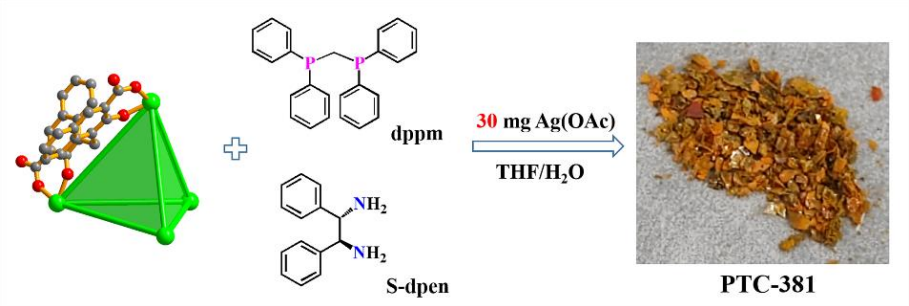

Scheme S4. The synthetic route of **PTC-381**.

X-ray Crystallography. Crystallographic data for **PTC-379** to **PTC-381** were collected on a Supernova single-crystal diffractometer equipped with graphite-monochromatized Ga or Cu Kα radiation (λ = 1.3405 Å or 1.54184 Å) at 100 K or 293 K. Absorption correction was applied using SADABS.[2] Structure was solved by direct method and refined by full-matrix least-squares on F2 using SHELXTL.[3] In these structures, some cations and free guest molecules were highly disordered and could not be located. The diffused electron densities resulting from these residual cations and guest molecules were removed from the data set using the SQUEEZE routine of PLATON[4] and refined further using the data generated. Crystal data and details of data collection and refinement of **PTC-379** to **PTC-381** were summarized in Table S1. CCDC (2360057-2360059) contain the supplementary crystallographic data for this paper. These data are provided free of charge by The Cambridge Crystallographic Data Centre.

Preparation of PTCs dispersed PDMS films. PTCs refers to compounds **PTC-379** to **PTC-381**. The crystals of these compounds need to be dried in the air before sampling. Firstly, 1 mg crystals was ground into fine powder in agate mortar, and then was mixed with 1.5 g PDMS (Sylgard 184, polydimethylsiloxane), and the sample was evenly dispersed by magnetic stirring for several hours. Secondly, 1/10 mass of specific curing agent was added into the mixture and continued to stir evenly for about 10 min. Thirdly, take 1 g of the mixture and put it into a specific membrane. Under the action of gravity, the mixture is paved in the mold, and then placed at room temperature for 0.5 hour to eliminate bubbles. Finally, put the membrane utensil into a 60 ℃ oven for 5h to obtain films for testing. In addition, we also tested these compounds in different dispersion concentrations. Using the same preparation method, 1mg, 2mg and 3mg crystals were used to make a film, respectively.

Z-scan Measurements. The third-order nonlinear optical (NLO) property of the samples was obtained using the open-aperture (OA) Z-scan technique. The excitation light source was an Nd:YAG laser with a repetition rate of 5 Hz. The laser pulses (period: 5 ns; wavelength: 532 nm) were split into two beams with a mirror. The pulse energies at the front and back of the samples were monitored using energy detectors D1 and D2. The sample was mounted on a computer-controlled translation stage that shifted each sample along the z-axis. All of the measurements were conducted at room temperature and under the same incident pulse energy of 100 μJ.

Z-scan data processing. The relationship of the sample transmission and input fluence can be plotted from the open-aperture Z-scan curve.[5,6] From the input laser pulse energy

E_{in} and beam radius $\omega(z)$, the light fluence $F_{in}(z)$ at any position can be obtained. $F_{in}(z)$ is defined as

$$F_{in}(z) = \frac{4E_{in}\sqrt{\ln 2}}{2a\pi^{\frac{3}{2}}\omega(z)^{2}}$$

Where $\omega(z)$ is defined as:

$$\omega(z) = \frac{\omega_0}{\left[1 + \left(\frac{z}{z_0}\right)^2\right]^{-\frac{1}{2}}}$$

where ω_0 and z_0 are the light beam radius and the Rayleigh range, respectively, and z_0 is defined as:

$$z_0 = \frac{k\omega_0^2}{2}$$

Where k is defined as:

$$k = \frac{2\pi}{\lambda}$$

The equation fits for the nonlinear adsorption coefficient β as follows:

$$T(Z, S = 1) = \frac{1}{\sqrt{\pi}q_0(z,0)}\int_{-\infty}^{\infty}\ln\left[1 + q_0(z,0)e^{-r^2}\right]dr$$

$$q_0(z,0) = \beta I_0 L_{eff}$$

$$L_{eff} = \frac{1 - e^{-\alpha l}}{a}$$

In these equations, I_0 is the on-axis peak intensity at the focus (Z = 0), L_{eff} is the effective thickness of the sample, α is the linear absorption coefficient, and l is the sample thickness.

References：

[1] Y. P. He, L. B. Yuan, G. H. Chen, Q. P. Lin, F. Wang, L. Zhang, J. Zhang, *J. Am. Chem. Soc*., 2017, **139**, 16845-16851.

[2] G. M. Sheldrick, SADABS, Program for area detector adsorption correction. *Institute for Inorganic Chemistry*, University of Göttingen, Göttingen (Germany), 1996.

[3] G. M. Sheldrick, SHELXL-2014/7: *A Program for Structure Refinement*, University of Göttingen, Göttingen, Germany, 2014.

[4] P. van der Sluis, A. L. Spek, *Acta Crystallogr. A.*, 1990, **46**, 194-201.

[5] J. Sun, B. Yuan, X. Hou, C. Yan, X. Sun, Z. Xie, X. Shao, S. Zhou, *J. Mater. Chem. C*., 2018, **6**, 8495-8501.

[6] L. Huang, C. Zheng, Q. Guo, D. Huang, X. Wu, L. Chen, *Opt. Mater.*, 2018, **76**, 335-343.

Table S1. Crystallographic Data and Structure Refinement Details for Compounds **PTC-379** to **PTC-381.**

Compound	**PTC-379**	**PTC-380**	**PTC-381**
CCDC	2360057	2360058	2360059
formula	$C_{285}H_{186}Ag_6N_{12}O_{36}P_6Ti_4$	$C_{212}H_{132}Ag_2N_4O_{36}P_4Ti_4$	$C_{294}H_{224}Ag_8N_8O_{36}P_8Ti_4$
formula weight	5379.09	3842.43	5747.12
crystal system	monoclinic	tetragonal	monoclinic
space group	*C*2/*c*	$P4_12_12$	*I*2/*a*
a (Å)	78.8953(7)	20.4503(4)	35.6145(4)
b (Å)	22.1894(2)	20.4503(4)	22.6414(2)
c (Å)	35.6493(3)	54.8956(15)	47.7519(7)
α (°)	90	90	90
β (°)	94.371(10)	90	110.160(2)
γ (°)	90	90	90
V (Å^3)	62227.6(9)	22958.1(11)	36146.2(9)
Z	8	4	4
D_{calcd} (g cm^{-3})	1.148	1.112	1.056
μ(Cu K*a*) (mm^{-1})	3.085	3.246	3.291
F(000)	21824.0	7848.0	11664.0
temperature (K)	99.99(10)	293(2)	99.99(10)
theta min, max (deg)	2.079, 56.381	2.306, 79.039	1.714, 56.362
tot., uniq. Data	308129/61135	114117/23543	281738/35521
R (int)	0.0681	0.0893	0.1501
observed data[($I > 2\sigma(I)$]	33333	11016	26485
N_{ref}, N_{par}	61135, 2977	23543, 1145	35521, 1601
R_1, wR_2 (all data)[a]	0.1253, 0.4053	0.0605, 0.2069	0.1090, 0.3120
S	1.354	0.934	1.077
Min and max resd dens (e·Å^{-3})	-1.21, 1.58	-0.33, 0.27	-1.38, 2.44

2. Detailed structural information.

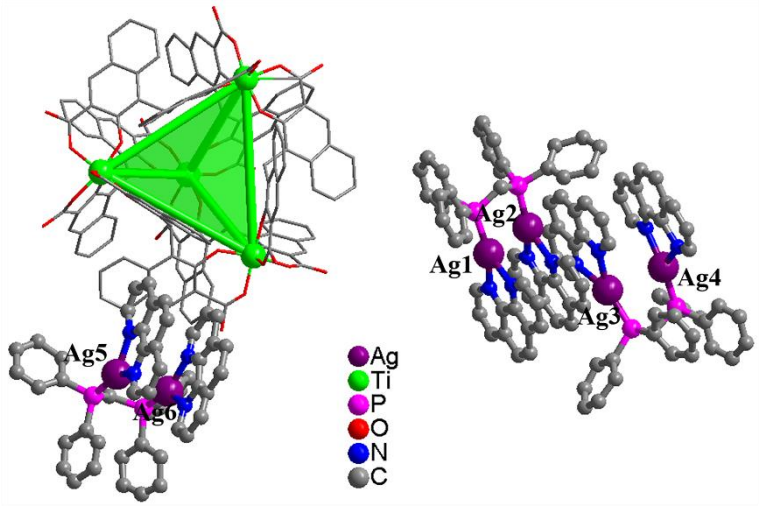

Figure S1. The asymmetric unit of **PTC-379**, showing one Ti_4L_6 cage and three $[Ag_2(phen)_2(dppm)]^{2+}$ cations (Solvents and $(Me_2NH_2)^+$ countercations could not be located because of highly disorder). Most H atoms have been removed for clarity. Atom color code: purple, Ag; green, Ti; pink, P; red, O; gray, C; off white, H.

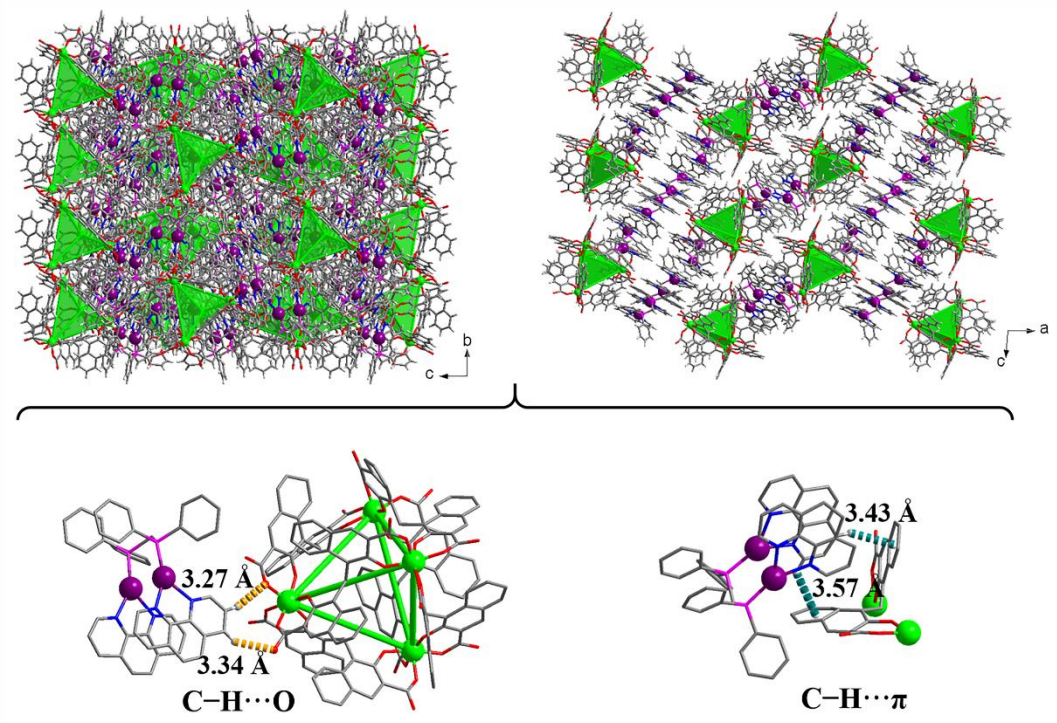

Figure S2. 3D packed framework of **PTC-379** and the supramecular interactions.

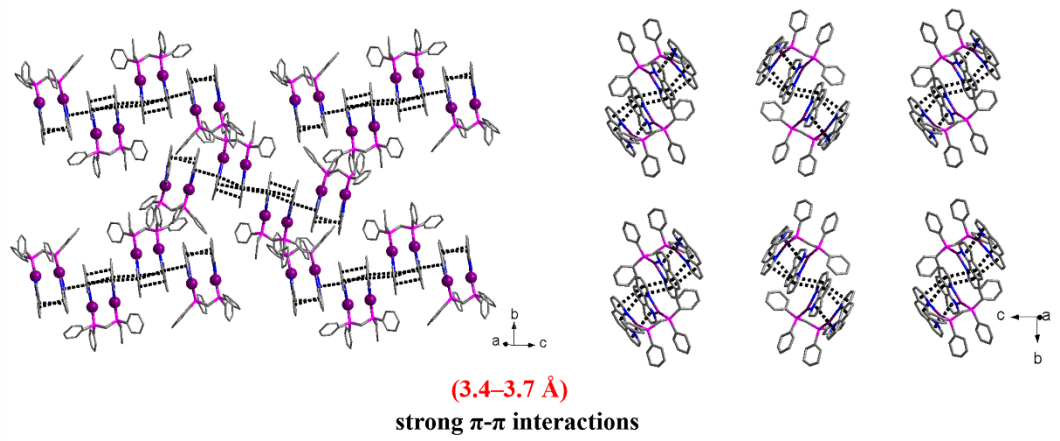

Figure S3. The highlighting of the π-π interactions between adjacent $[Ag_2(phen)_2(dppm)]^{2+}$ cations in **PTC-379**.

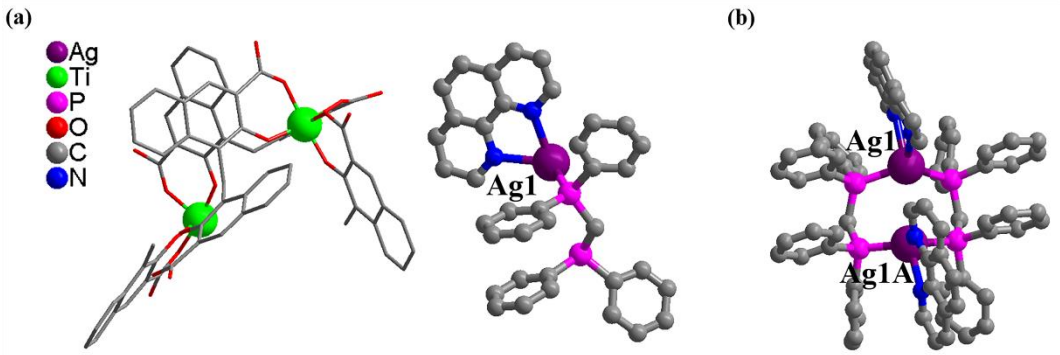

Figure S4. (a) The asymmetric unit of **PTC-380**, showing half of Ti_4L_6 cage and half of $[Ag_2(phen)_2(dppm)_2]^{2+}$ cations (Solvents and $(Me_2NH_2)^+$ countercations could not be located because of highly disorder). (b) The $[Ag_2(phen)_2(dppm)_2]^{2+}$ unit. Most H atoms have been removed for clarity. Atom color code: purple, Ag; green, Ti; pink, P; red, O; gray, C; off white, H.

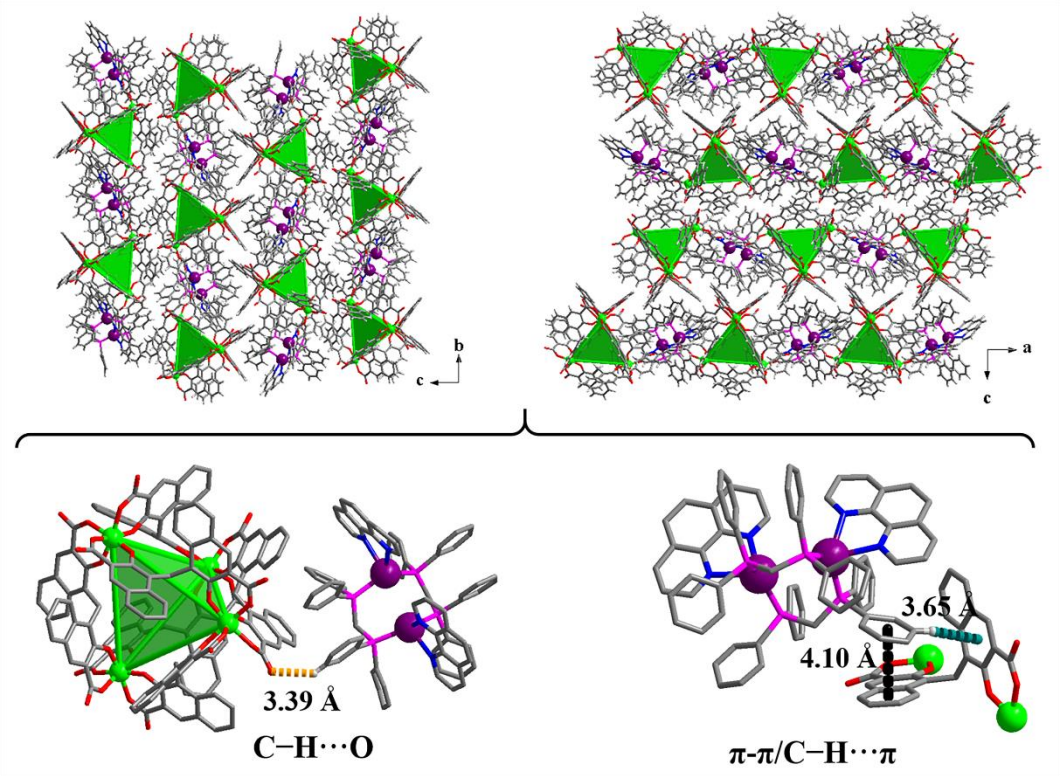

Figure S5. 3D packed framework of **PTC-380** and the supramecular interactions.

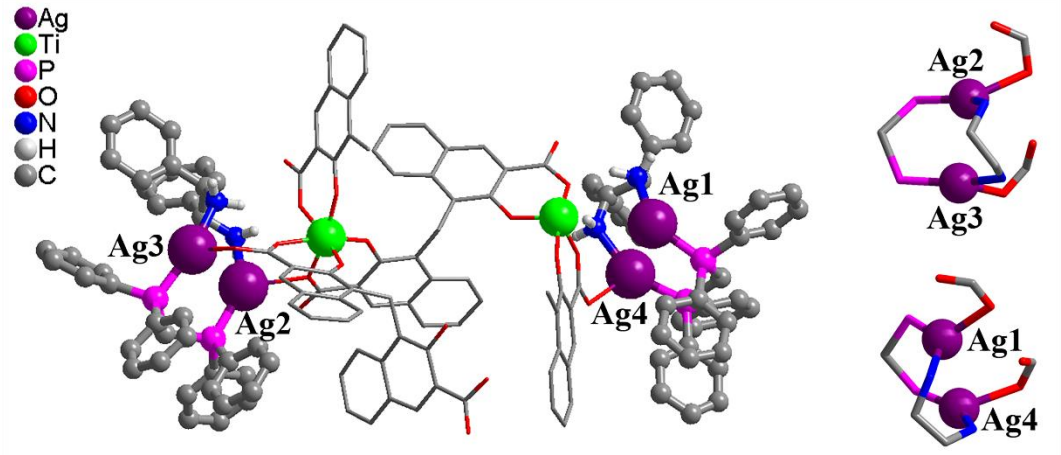

Figure S6. The asymmetric unit of **PTC-381**, showing half of Ti_4L_6 cage and two coordinated $[Ag_2(S\text{-dpen})(dppm)]^{2+}$ cations (Solvents could not be located because of highly disorder). Most H atoms have been removed for clarity. Atom color code: purple, Ag; green, Ti; pink, P; red, O; gray, C; off white, H.

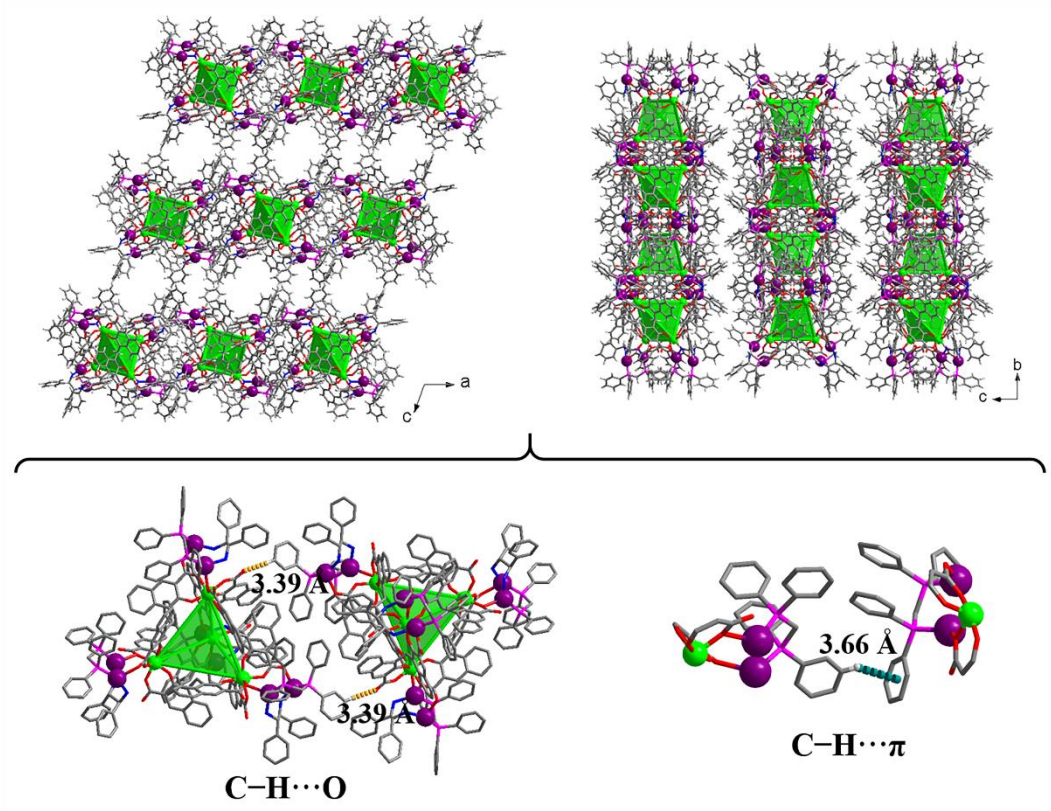

Figure S7. 3D packed framework of **PTC-381** and the supramecular interactions.

3. TG, PXRD and UV data.

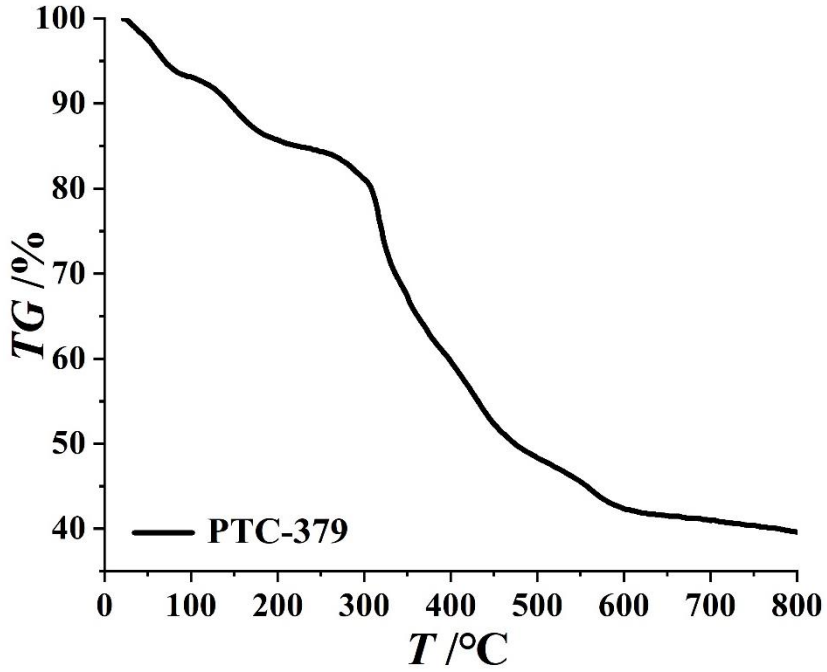

Figure S8. The TGA curve of **PTC-379**.

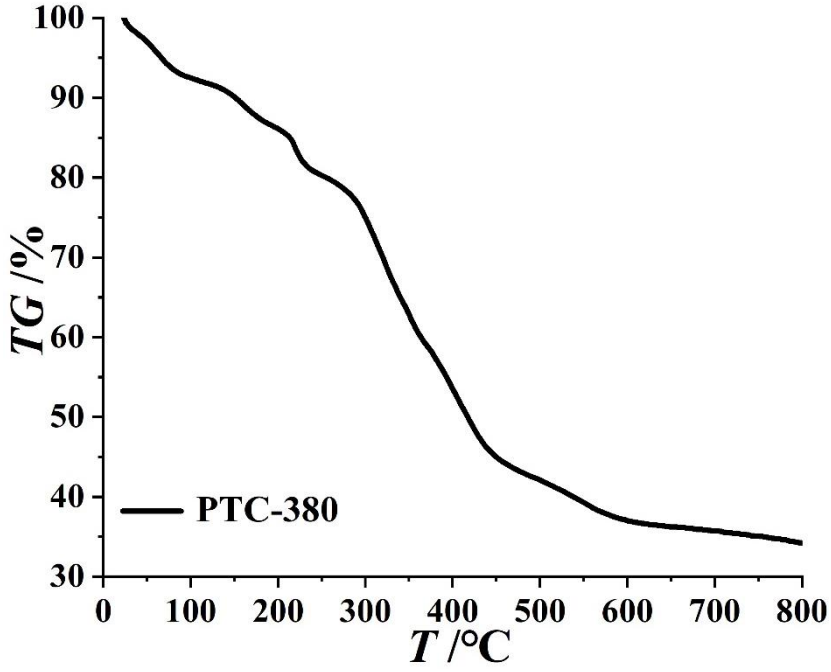

Figure S9. The TGA curve of **PTC-380**.

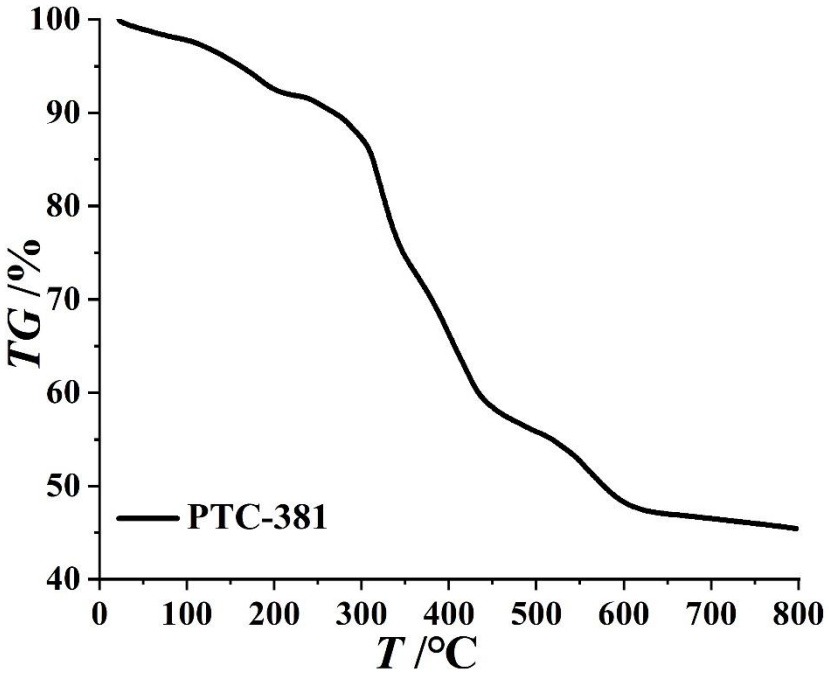

Figure S10. The TGA curve of **PTC-381**.

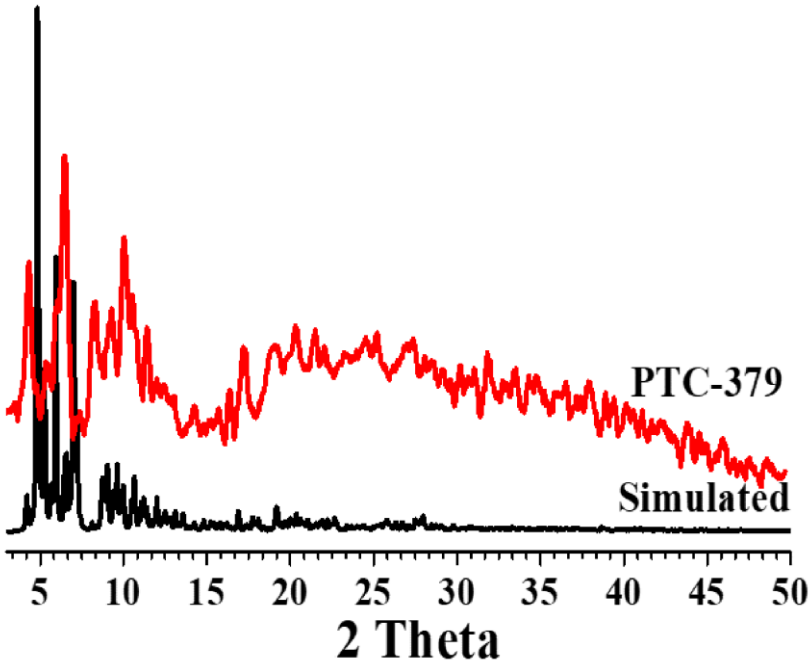

Figure S11. PXRD patterns of simulated from the single-crystal data of **PTC-379** (black) and as-synthesized **PTC-379** (red).

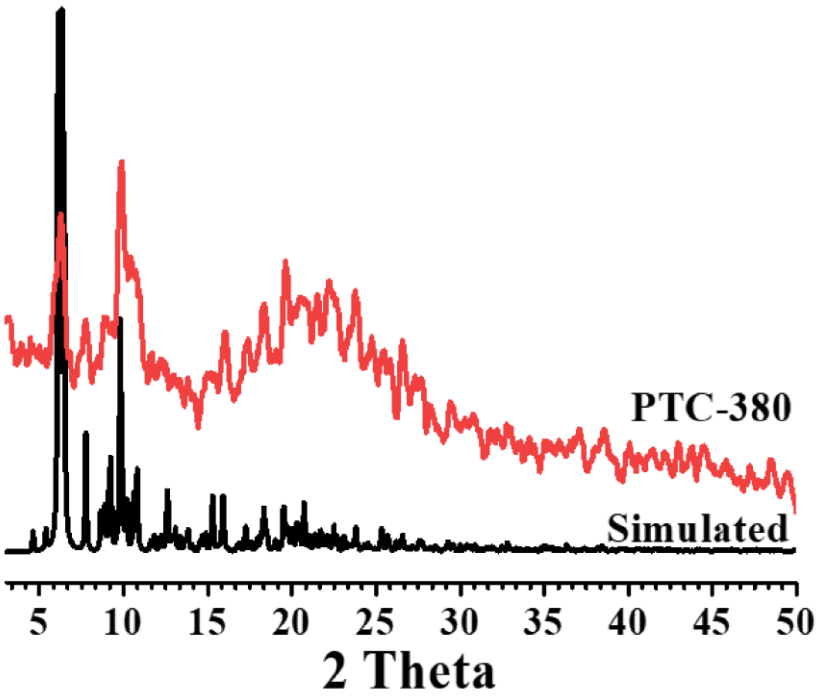

Figure S12. PXRD patterns of simulated from the single-crystal data of **PTC-380** (black) and as-synthesized **PTC-380** (red).

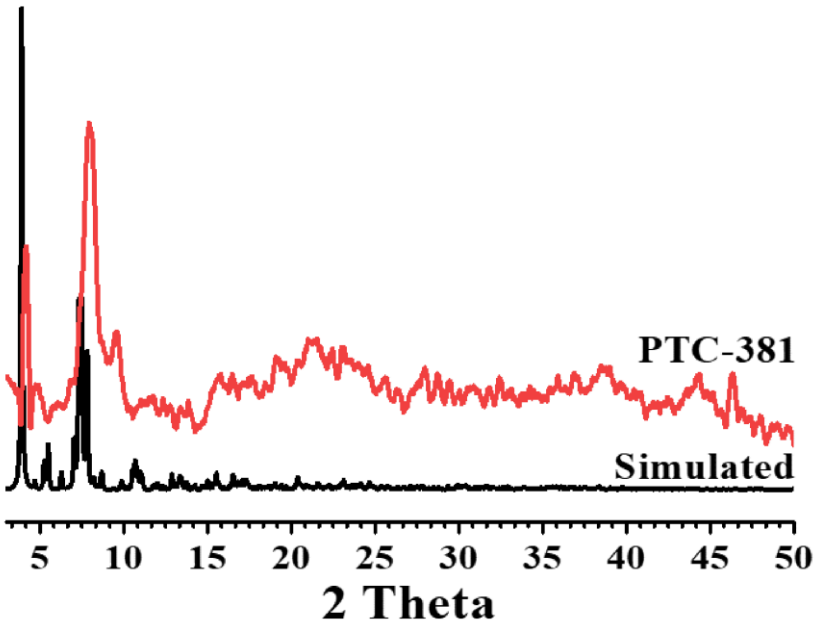

Figure S13. PXRD patterns of simulated from the single-crystal data of **PTC-381**(black) and as-synthesized **PTC-381** (red).

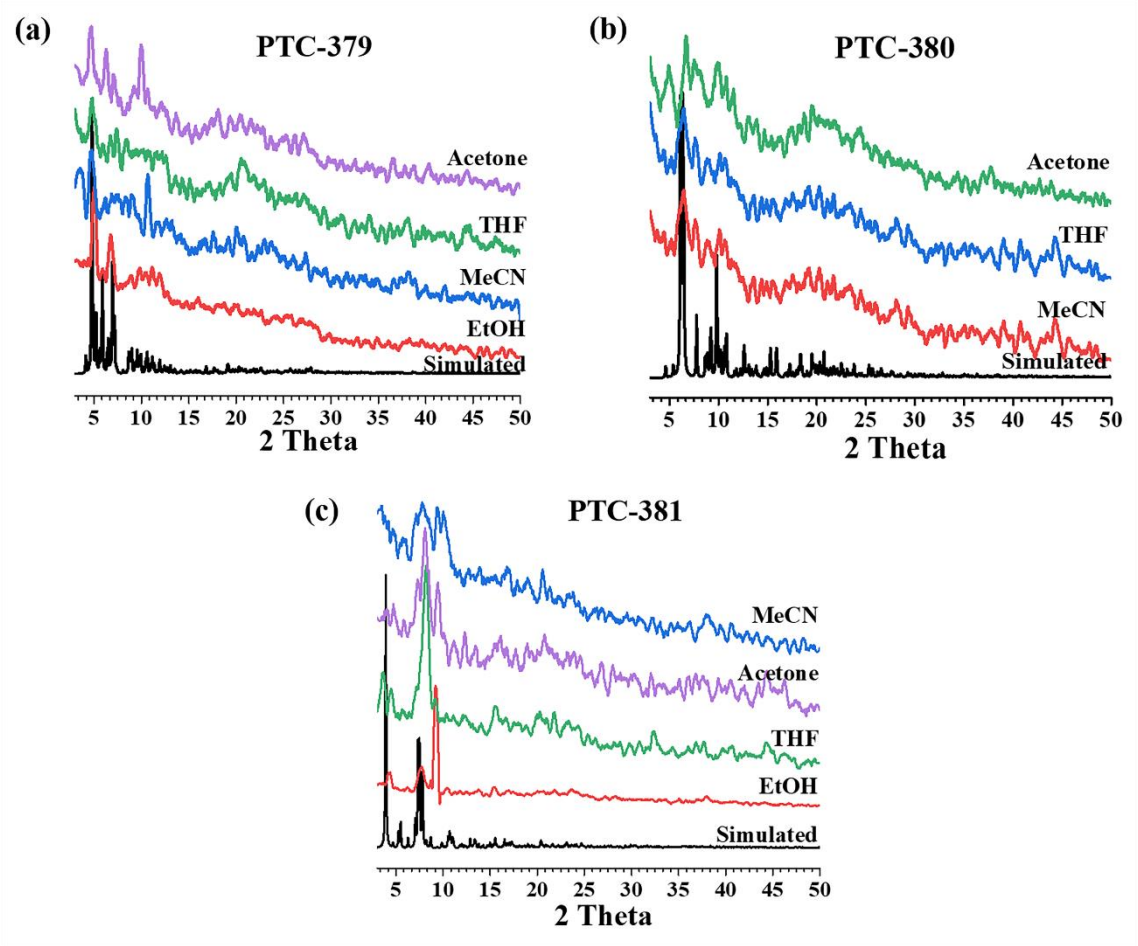

Figure S14. Solvent stability study for **PTC-379** (a), **PTC-380** (b) and **PTC-381** (c).

The PXRD pattern was obtained after immersing crystals of **PTC-379** to **PTC-381** in different solvents for 12h, respectively. As shown in Figure S14, the results show that **PTC-379** can be stable in EtOH and acetone, because their PXRD peaks match well with the simulated one, but it has relative poor stability in THF and MeCN. For **PTC-380**, it has good stability in MeCN, THF and acetone, but it can be soluble in EtOH. For **PTC-381**, it can be stable in EtOH, THF and acetone, but it has relative poor stability in MeCN. In addition, all the crystals of **PTC-379** to **PTC-381** were found to be soluble in DMF.

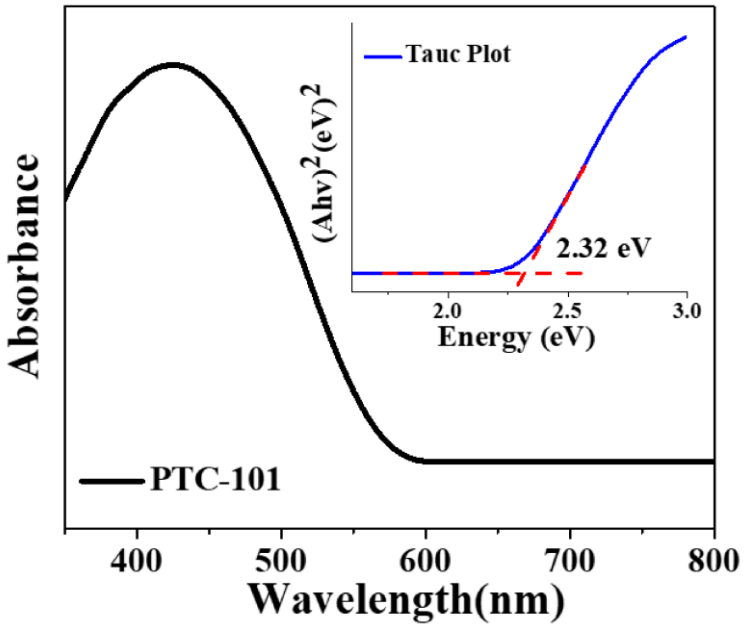

Figure S15. Solid-state UV absorption spectrum of PTC-101.

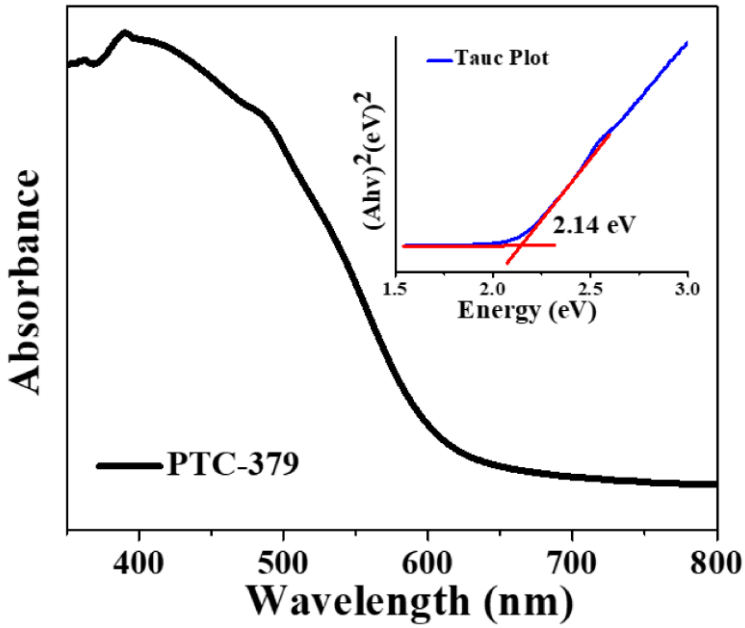

Figure S16. Solid-state UV absorption spectrum of **PTC-379**.

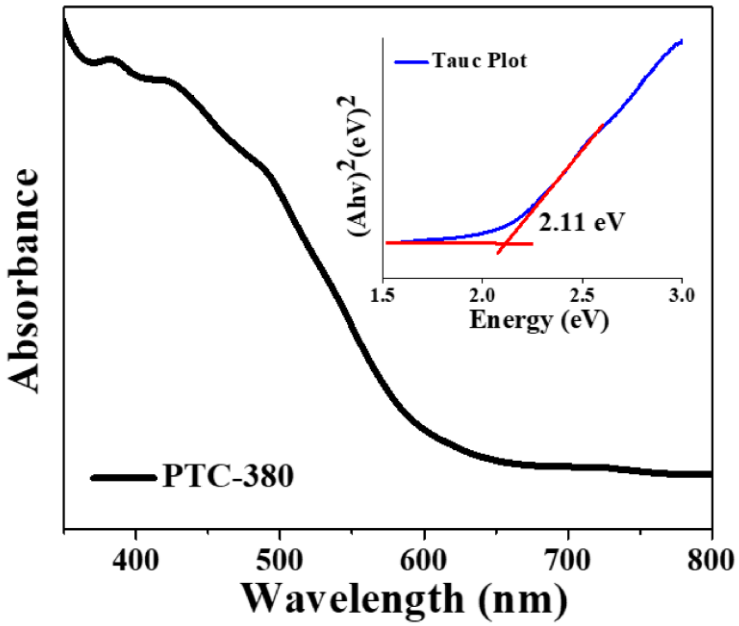

Figure S17. Solid-state UV absorption spectrum of **PTC-380**.

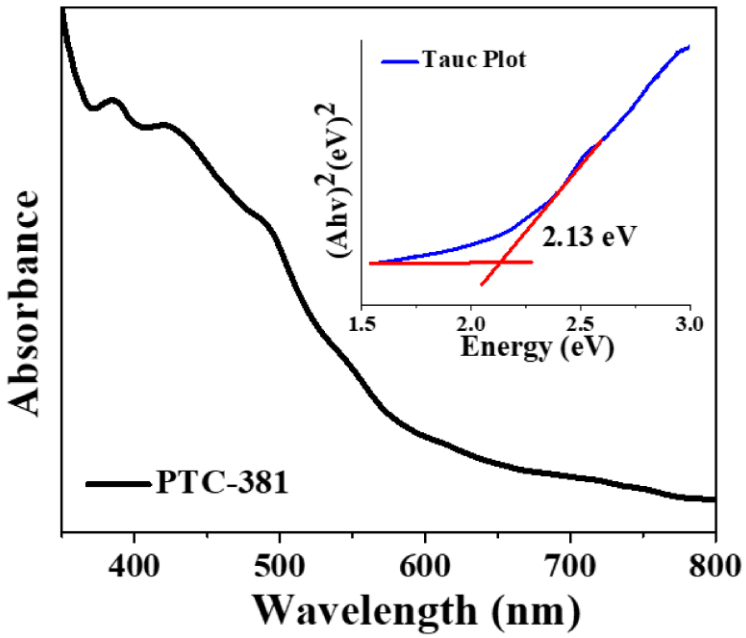

Figure S18. Solid-state UV absorption spectrum of **PTC-381**.

4. Third-order nonlinear optical (NLO) property study.

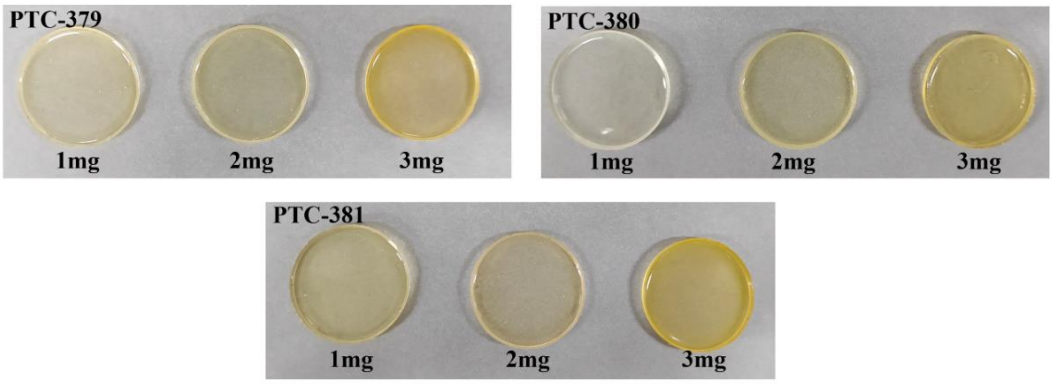

Figure S19. The photos of PDMS-PTCs films.

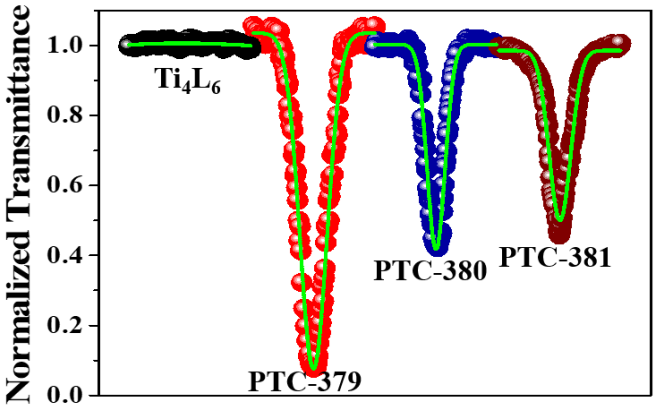

Figure S20. OA Z-scan (points) and theoretical fit (solid lines) curves of **PDMS-PTCs** films and the starting material (Ti_4L_6 cage) at 532 nm.

The experimental results show that all the **PDMS-PTCs** films exhibit a typical reverse saturation absorption (RSA) behavior, revealing notable optical limiting effects. At Z=0, the minimum normalized transmission (T_{min}) of **PDMS-PTC-379**, **PDMS-PTC-380** and **PDMS-PTC-381** are 0.08, 0.42 and 0.46, respectively (Figure S20). For better comparison, we also tested third-order NLO properties of Ti_4L_6 starting material (PDMS-PTC-101) using the same thin film preparation method. Obviously, it has no obvious optical limiting effect. The β value of **PDMS-PTC-379**, **PDMS-PTC-380** and **PDMS-PTC-381** is 22.09, 2.89 and 2.30 $\times 10^{-9}$ m W^{-1}, and the optical limiting threshold (F_{OL}) of them is 0.08 J cm^{-2}, 1.20 and 2.75 J cm^{-2}, respectively. By comparison, it is found that **PDMS-PTC-379** has the highest β value and the lowest F_{OL} value, indicating its high NLO performance, which can be contributed to the rich and strong π-π stacking

interactions in its structure (Figure S3).

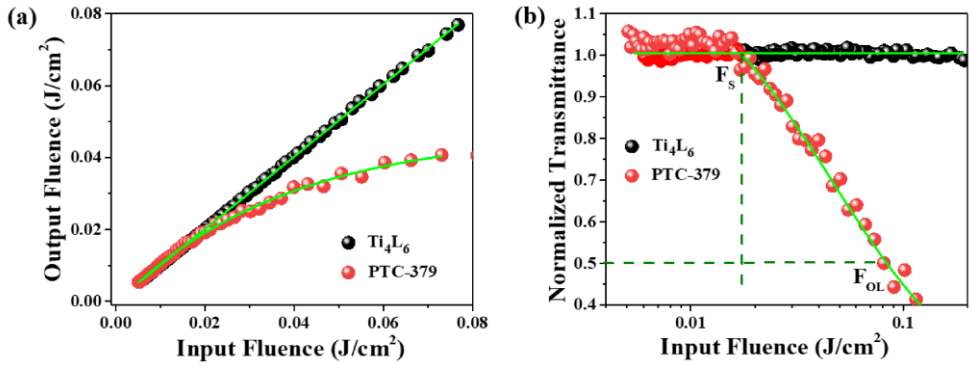

Figure S21. (a, b) The curves of output fluence versus input fluence for PDMS-PTC-101 and **PDMS-PTC-379** films, and variation in the normalized transmittance as a function of input intensity for them.

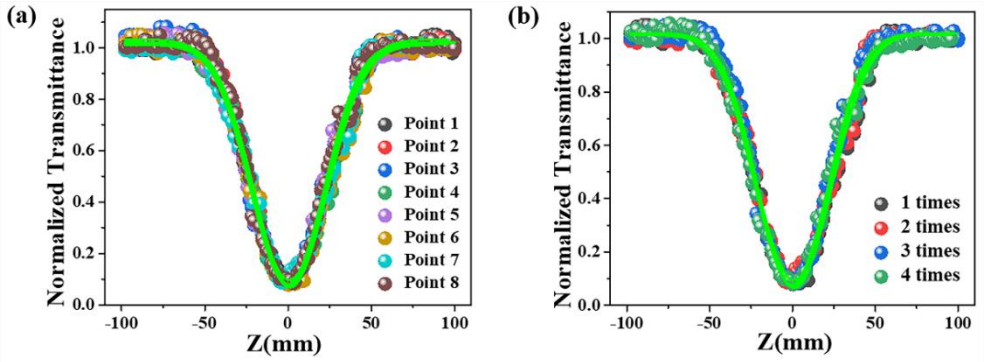

Figure S22. (a, b) The same **PDMS-PTC-379** film is tested at different points and at the same point, respectively.

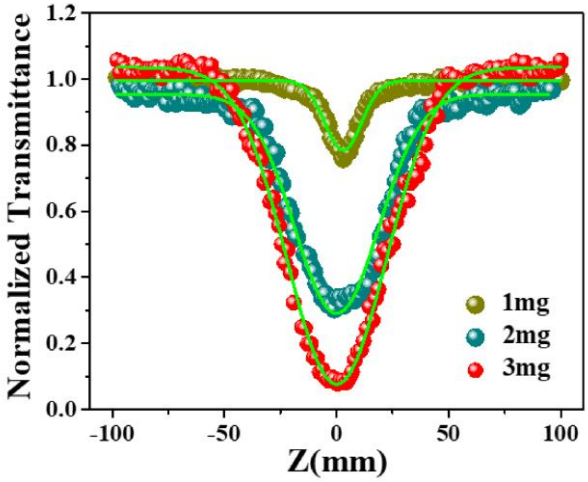

Figure S23. NLO responses at different concentrations of **PTC-379**.

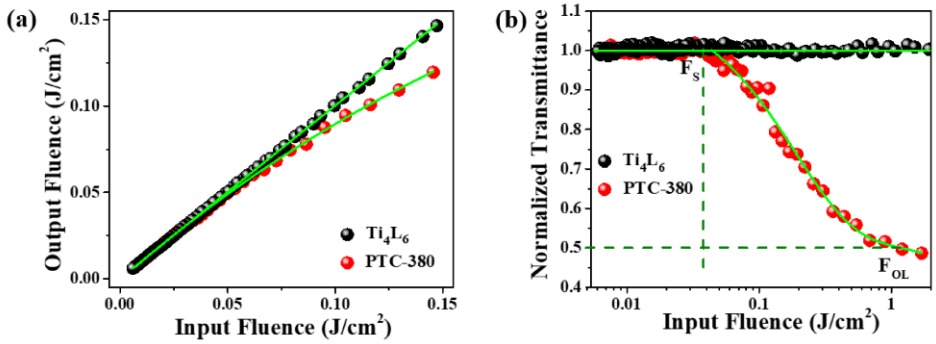

Figure S24. (a, b) The curves of output fluence versus input fluence for PDMS-PTC-101 and **PDMS-PTC-380** films, and variation in the normalized transmittance as a function of input intensity for them.

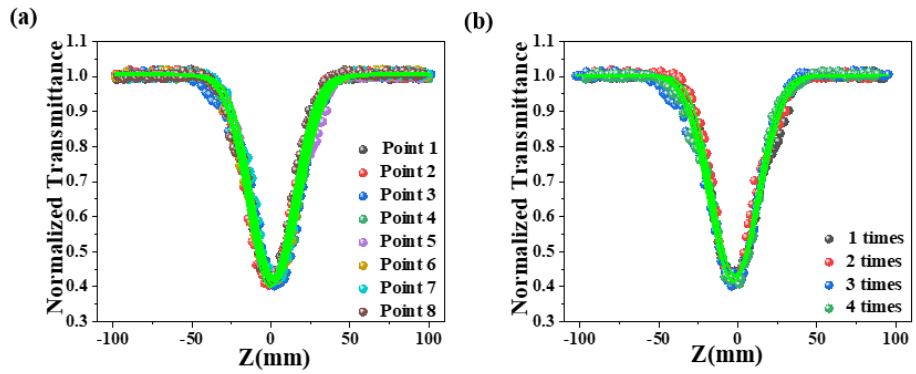

Figure S25. (a, b) The same **PDMS-PTC-380** film is tested at different points and at the same point, respectively.

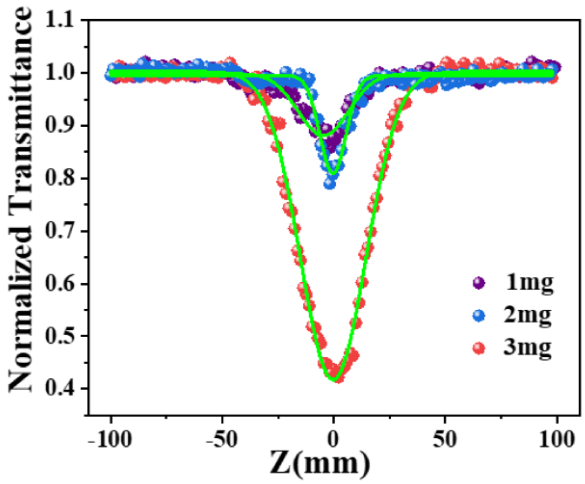

Figure S26. NLO responses at different concentrations of **PTC-380**.

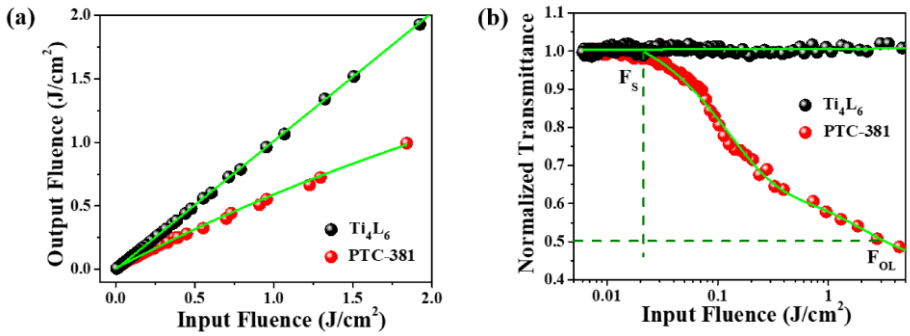

Figure S27. (a, b) The curves of output fluence versus input fluence for PDMS-PTC-101 and **PDMS-PTC-381** films, and variation in the normalized transmittance as a function of input intensity for them.

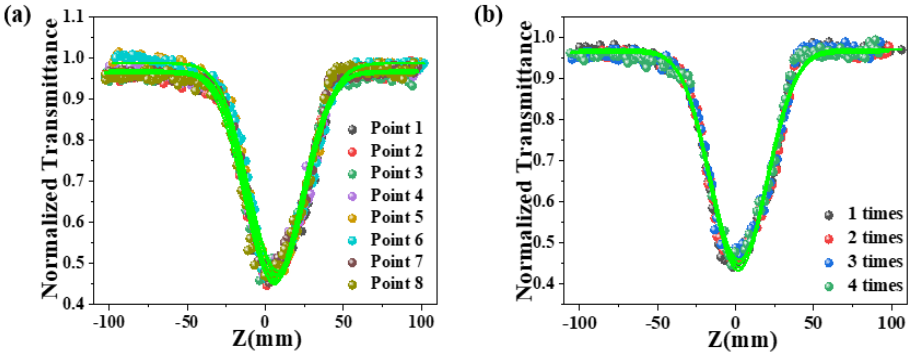

Figure S28. (a, b) The same **PDMS-PTC-381** film is tested at different points and at the same point, respectively.

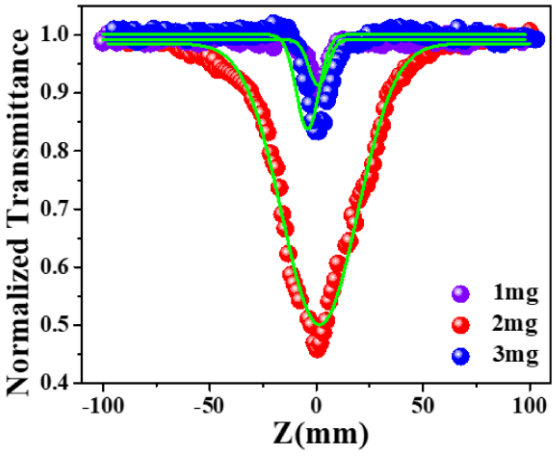

Figure S29. NLO responses at different concentrations of **PTC-381**.

5. Density function theory (DFT) calculation.

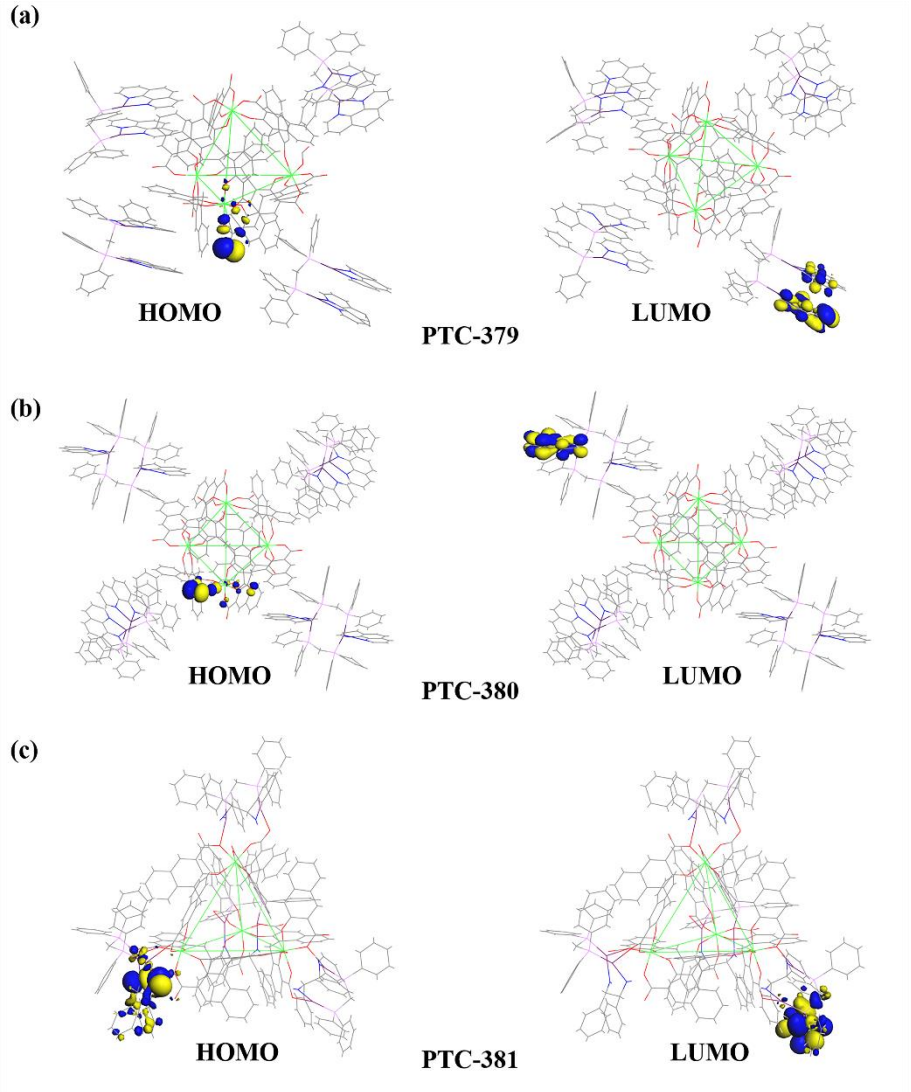

Figure S30. The frontier molecular orbitals theoretical views of the HOMO and LUMO states of **PTC-379** (a), **PTC-380** (b) and **PTC-381** (c) that were obtained from the DFT calculations.

In order to better understand the structure–activity relationship, the density function theory (DFT) was used to calculate the electronic properties and frontier orbitals of **PTC-379** to **PTC-381** (Figure S30). For the ion pair structures **PTC-379** and **PTC-380**, the results show that the contribution of HOMO comes from the anionic Ti_4L_6 cage and the LUMO from the π orbitals of Ag_2 coordination cations, respectively. For the modified structure **PTC-381**, the HOMO is mainly provided by the S-dpen ligand, and the LUMO is mainly provided by the dppm ligand. The electron transfers between HOMO and LUMO are mainly ligand-to-ligand charge transition (LLCT).

Computational methods. All density functional theory calculations were implemented by the Dmol^3 package.[1] All calculations were performed with PBE exchange-correlation functional on **PTC-379** to **PTC-381**.[2] The double-numeric quality basis set with polarization functions (DNP) was adopted.[3] The numerical basis sets can minimise the basis-set superposition error.[4] A Fermi smearing of 0.005 hartree was utilized, and the tolerances of the energy, gradient and displacement convergence were 1 $\times 10^{-5}$ hartree, 2 $\times$ 10^{-3} hartree per Å, and 5 $\times 10^{-3}$ Å, respectively.

References：

[1] S. Grimme, J. Antony, S. Ehrlich, H. Krieg, *J. Chem. Phys.*, 2010, **132**, 154104.

[2] J. P. Perdew, K. Burke, M. Ernzerhof, *Phys. Rev. Lett.*, 1996, **77**, 3865-3868.

[3] U. V. Barth, L. Hedin, *J. Phys. C: Solid State Phys.*, 1972, **5**, 1629-1642.

[4] N. Matsuzawa, J. e. Seto, D. A. Dixon, *J. Phys. Chem. A*, 1997, **101**, 9391-9398.